Use of colour transformation and the geodesic method for road centreline extraction from VHR satellite images

ZELANG MIAO[a b *], LIPENG GAO[c d], YUEGUANG HE[e *], LIXIN WU[a b], WENZHONG SHI[d], ALIM SAMAT[f], SICONG LIU[g], and JIA LI[a b]

[a] School of Geosciences and Info-Physics, Central South University, Changsha 410083, China

[b] Key Laboratory of Metallogenic Prediction of Nonferrous Metals and Geological Environment Monitoring, Central South University, Changsha 410083, China

[c] School of Remote Sensing and Information Engineering, Wuhan University, Wuhan 430079, China

[d] Department of Land Surveying and Geo-Informatics, The Hong Kong Polytechnic University, Kowloon, Hong Kong

[e] School of Traffic and Transportation Engineering, Changsha University of Science Technology, Changsha 410083, China

[f] Xinjiang Institute of Ecology and Geography, State Key Laboratory of Desert and Oasis Ecology No818, South Beijing Road, Urumqi 830011, Xinjiang, China

[g] College of Surveying and Geo-informatics, Tongji University, Shanghai 200092, China

Seed point based road extraction methods are vital for extracting road networks from satellite images. Despite its effectiveness, roads in very high-resolution (VHR) satellite images are complicated, such as road occlusion and material change. To tackle this issue, this paper proposes to use the colour space transformation and geodesic method. First, the test image is converted from Red-Green-Blue colour space to Hue-Saturation-Value colour space to reduce the material change influence. The geodesic method is subsequently applied to extract initial road segments that link road seed points provided by users. At last, the initial result is adjusted by a kernel density estimation method to produce centred roads. The presented method is quantitatively evaluated on three test images. Experiments show that the proposed method yields a substantial improvement over cutting-edge technologies. The findings in this study shine new light on a practical solution for road extraction from satellite images.

1. Introduction

With the advent of Very High Resolution (VHR) imaging satellite systems, the number of images grows larger and larger, efficient and accurate image interpretation and analysis have become a crucial requirement for a variety of tasks. Among all these tasks, road delineation from VHR satellite images plays an indispensable role in many practical applications. Road delineation has received much attention over the years and there are many methods designed from different prospective. In contemporary literature, there are two main types of algorithms for road extraction (Mena 2003; Poullis and You 2010; Das, Mirnalinee, and Varghese 2011): fully automatic and semi-automatic methods. Fully automatic methods are an interesting and attractive topic that has been

* Corresponding author. Email: zelang.miao@csu.edu.cn, hyg@csust.edu.cn.

researched for decades. However, though sustained research, results of fully automatic methods are very subjective (Turetken et al. 2011), since the nature scenes are generally particularly complicated, such as road material change, tree and shadow occlusion. Therefore, due to the limited accuracy, fully automatic road delineation from satellite images still remains open and challenging (Dal Poz et al. 2012).

This study focuses on developing a semi-automatic road extraction method. Road extraction methods were founded on diverse image processing technologies. By integrating photometric and geometric features, roads are models in the object-space using stereoscopic aerial images (Dal Poz et al. 2012). After that, the road network is iteratively constructed by dynamic programming. Based on a piecewise parabola model with 0-order, a semi-automated road extraction was designed (Hu, Zhang, and Tao 2004). This method relies on the seed points provided by users to construct the piecewise parabola model, followed by the solving each piece of parabola using image constraints based on a least square template matching. An interlaced template matching (Lin et al. 2011) based on the least square is developed for urban road extraction from VHR satellite images. This method firstly constructs an interlaced reference template based on road seed points. The reference template is then convolved with the image, followed by road axis tracing based on the least squares template. Similarly, the template matching is combined with distance transformation to extract roads in urban areas (Zhang et al. 2011). Some researchers proposed to treat road seed point connection as a shortest-path problem to improve the efficiency of road extraction on the basis of seed points. Lv et al. (2017) proposed a multi-feature sparsity-based model that can utilize multi-feature complementation to extract roads from high-resolution imagery (Lv et al. 2017). To maintain road-point connectivity, an edge-constraint fast marching method was proposed to sequentially link discrete seed points (Gao et al. 2018). Chai et al. (2013) extended the original idea of sampling line segments and built a graph model of road network through road nodes. Its disadvantage is that that correspond computational cost of the corresponding objective function is very expensive and may not be able to find a satisfactory optimum (Chai, Forstner, and Lafarge 2013). Road network structures were also represented as probabilistic graph, it extracted the road network as selecting the optimal subset of candidate paths, which is posed as MAP inference in a higher-order conditional random field (Wegner, Montoya-Zegarra, and Schindler 2015). Recently, the geodesic method (Peyr et al. 2010) is becoming a hot spot in the field of computer vision. This method relies on the local metric that encodes rich information to solve the connection issue between two selected points. A kernel density estimation method combined with the geodesic method is proposed to decrease the number of seed points required for road extraction (Miao et al. 2014). Although the geodesic method shows its advantages in road connection, however, it is not suitable for tracing roads where material change occurs. Meanwhile, the geodesic method result is not centred, and hence there is still large room to improve its accuracy.

In this paper, a semi-automatic method for road delineation from VHR satellite images is proposed method. The objective of this method is to develop a robust and general tool that can provide a practical solution for semi-automatic road extraction.

2. Methodology

The proposed method aims to devise a semi-automatic and efficient approach that can cope with road material change issue to extract road centreline from VHR satellite images. Figure 1 summarizes the proposed method.

Figure 1 here

The proposed method consists of three main steps, as follows:

Step 1: Perform colour transformation.

Step 2: Connect the seed points provided by users. The connection result is taken as the initial road centreline. Take the initial road centreline as the initial mask to implement level set to extract road segments around the initial road centreline.

Step 3: Adjust the initial road centreline to produce the centred road network.

Details of each step are described in the following sections.

2.1 Colour transformation

The major difficulty of many road extraction methods is the variability of the colour values in the Red-Green-Blue (*R, G, B*) colour space due to illumination changes caused by many factors, such as material change, image noise. Therefore, the *R, G, B* colour space needs to be transformed into another colour space to reduce the negative influence of illumination change. In other words, colour invariants are required for robust road detection. To this end, *R, G, B* colour space is converted to *H, S, V* (i.e. Hue, Saturation, and Value) colour space (Gonzalez, Woods, and Eddins 2003) using the following set of equations:

$$V = \max(R,G,B) \tag{1}$$

$$S = \begin{cases} \dfrac{V - \min(R,G,B)}{V}, V \neq 0 \\ 0, V = 0 \end{cases} \tag{2}$$

If $S = 0$, then

$$H = 0 \tag{3}$$

If $R = V$, then,

$$H = \begin{cases} \dfrac{60(G - B)}{V - \min(R,G,B)}, G \geq B \\ 360 + \dfrac{60(G - B)}{V - \min(R,G,B)}, G < B \end{cases} \tag{4}$$

If $G = V$, then,

$$H = 120 + \frac{60(B - R)}{V - \min(R, G, B)} \tag{5}$$

If $B = V$, then,

$$H = 240 + \frac{60 * (R - B)}{V - \min(R, G, B)} \tag{6}$$

An example of colour transformation is given in Figure 2. The original RGB image is shown in Figure 2(a) and its corresponding Hue (*H*), Saturation (*S*), and Value (*V*) are shown in Figures 2(b)-2(d). This image will be used through the whole study to visualize the computation steps. Figure 2(a) shows that the test image contains two different road types, whose spectral response values are different. By contrast, the illumination change caused by road material change is mostly eliminated after colour transformation, as shown in Figure 2(c).

Figure 2 here

2.2. Connection of road seed points

After the colour transformation, the road seed points placed by users are linked by the geodesic method (Peyr et al. 2010) to create the central line, which in turn formulates the road network. For 2D case, let $\Omega = [0,1]^2$ denote the image domain and $\gamma(t) : [0,1] \to \Omega$ be a smooth curve on the image I where t is the curve parameter. Suppose $\boldsymbol{x}_0$ and $\boldsymbol{x}_1$ are starting and ending points of $\gamma(t)$, which can be expressed as

$$\{\gamma(t) : [0,1] \to \Omega \setminus \gamma(0) = x_0 \text{ and } \gamma(1) = x_1\} \tag{7}$$

Suppose $L(\gamma)$ be the weighted length of $\gamma(t)$, which can be computed by the integrating method.

$$L(\gamma) = \int_0^1 W(\gamma(t)) \| \gamma'(t) \| \, \mathrm{d}t \tag{8}$$

where $W(\cdot)$ is a weight function, and $\gamma'(t) \in \square^2$ is the derivative of $\gamma(t)$.

This study assumes that roads can be approximately modelled as a smooth curve that has a constant grey value of $c \in \square$. Based on this road model assumption, a weight function $W(\boldsymbol{x})$ can be defined as

$$W(x) = |I(x) - c| + \varepsilon \tag{9}$$

where ε (i.e., $\varepsilon = 0.01$) is a small value that guarantees $W(x)$ be non-zero. In this

study, the constant value c is fixed to $I(\boldsymbol{x}_0)$. The road that links $\boldsymbol{x}_0$ and $\boldsymbol{x}_1$ are taken to be a curve γ^* that has the minimal length between all possible curves between $\boldsymbol{x}_0$ and $\boldsymbol{x}_1$.

$$\gamma^* = \min_{\gamma \in (x_0, x_1)} L(\gamma) \tag{10}$$

where γ^* is called the minimal path.

Figure 3(a) shows an example of linking the end points by using the geodesic method on the original RGB image. It can be seen that grey values of two seed points are very large, owing to the road material change issue. This issue makes the geodesic method fail to connect seed points with desired spatial topology. By contrast, the geodesic method correctly traces roads between two seed points based on the saturation image produced by colour transformation, as shown in Figure 3(b). This example demonstrates the advantage of colour transformation in road connection problem. Despite the efficiency, it is worth pointing out that the geodesic method inclines to trace roads along the boundary, which departs from the text the centreline (see Figure 3(c)). In other words, the geodesic result is not precisely coinciding with the road centreline.

Figure 3 here

2.3. Adjustment of the connection result

The purpose of *Step 2.3* is to adjust the initial coarse road centreline to produce accurate result that precisely locates on the road centreline. To do so, the buffer around the road centreline is firstly constructed. For each pixel in the buffer, its probability that locates on the centreline is subsequently estimated based on kernel density estimation (KDE). Finally, the geodesic method is applied again on the KDE result to produce accurate road centreline.

Generally speaking, the road width is not consistent in real case, and hence the road buffer should be adaptively changed where the road width changes. Meanwhile, the buffer should contain the minimum *non-road* pixels. The buffer around the initial road centreline can be seen as the object and extracted by finding an optimal contour C by the energy function $E(C)$ defined as

$$E(C) = \lambda |C| + \int_{C_{\text{in}}} |x_i - \mu_{\text{in}}|^2 \, \mathrm{d}x\mathrm{d}y + \int_{C_{\text{out}}} |x_i - \mu_{\text{out}}|^2 \, \mathrm{d}x\mathrm{d}y \tag{11}$$

where λ is the smoothing term that serves as the penalty term to penalize the evolving contour curve length and keep the curve smooth, $|C|$ denotes the contour length, x_i is the ith pixel grey value, C_{in} and C_{out} are foreground and background,

respectively, and μ_{in} and μ_{out} are the corresponding intensity mean grey values of C_{in} and C_{out}, respectively. The contour is subsequently evolved to fit the edges of objects by making Equation (11) reach a minimum value. To this end, level set (Osher and Fedkiw 2001; Vese and Chan 2002) is developed to minimize the energy function $E(C)$. Let Ω represent the image domain and the curve C is represented by the zero level set of Lipchitz function φ, such that

$$\begin{cases} \varphi(x,y) > 0 & (x,y) \in C_{\text{in}} \\ \varphi(x,y) = 0 & (x,y) \in C \\ \varphi(x,y) < 0 & (x,y) \in C_{\text{out}} \end{cases} \tag{12}$$

The Heaviside step function H and Dirac delta function δ are then introduced to describe the functional as follows:

$$H(z) = \begin{cases} 1 & z \geq 0 \\ 0 & z < 0 \end{cases} \tag{13}$$

$$\delta(z) = \frac{\mathrm{d}}{\mathrm{d}z} H(z) \tag{14}$$

By instituting the unknown variable C by level set function φ, Equation (11) can be rewritten as

$$\begin{aligned} E(\varphi) = \lambda \int_{\Omega} \delta(\varphi) |\nabla \varphi| \mathrm{d}x\mathrm{d}y + \int_{\Omega} |x_i - \mu_{\text{in}}|^2 H(\varphi) \mathrm{d}x\mathrm{d}y \\ + \int_{\Omega} |x_i - \mu_{\text{out}}|^2 (1 - H(\varphi)) \mathrm{d}x\mathrm{d}y \end{aligned} \tag{15}$$

where $\nabla \varphi$ is the gradient of φ. Equation (15) is iteratively implemented until the optimal φ is produced. For computational details, we refer the readers to the biography written by Chan and Vess (2001).

After the road buffer construction, the kernel density estimation (KDE) technology (Ahamada and Flachaire 2010) is introduced to assess the probability that a pixel lies on the road centreline. Let $X_1, X_2, \cdots, X_n$ be a given set of pixels which are in the road buffer. The kernel density estimator is defined as

$$\hat{f}(X) = \frac{1}{nh^d} \sum_{i=1}^{n} K\left(\frac{X - X_i}{h} \right) \tag{16}$$

where h denotes the bandwidth parameter, d is the data dimension and K is the kernel function. This study selects the Gaussian kernel as the kernel function. The Gaussian kernel is defined as

$$K(X) = e^{-\frac{X^2}{2h^2}} \tag{17}$$

The bandwidth parameter h is determined by:

$$h = \frac{1}{n^{d+4}} \boldsymbol{\Sigma}^{1/2} \tag{18}$$

where n is the number of data, $\boldsymbol{\Sigma}$ is the covariance matrix of data (Scott 2015).

An example of KDE is depicted in Figure 4. The *road* class map is shown in Figure 4(a) and its corresponding KDE result is illustrated by Figure 4(b). As hinted by Figure 4(b), pixels on road centreline have higher KDE values than pixels that are un-centred. The geodesic method is implemented on the KDE map to connect road seed points. The connection result is shown in Figure 4(c). Compared Figure 3(c) and Figure 4(c), it can be seen that the connection result on KDE is more centred than the result on the original RGB image.

Figure 4 here

3. Test Cases

In this section, several experiments are conducted to test the proposed method performance. The proposed method is also compared with other methods studied in the literature to show the method's advantages or disadvantages.

3.1 Datasets

To assess the effectiveness and adaptability of the presented method, experiments were conducted with three VHR remote sensing images. The images are described below.

The first image has a spatial resolution of 0.6 m/pixel and a spatial size of 512 pixels × 512 pixels and shows an area that is mainly covered by vegetation, roads, and buildings. It was collected by the QuickBird satellite and was downloaded from VPLab [46]. The image is shown in Figure 5(a).

The second image is shown in Figure 5(b) and has a spatial size of 3000 pixels × 1854 pixels and a spatial resolution of 2.5m /pixel. It was collected by the SPOT-5 satellite and shows an area of Melbourne, Australia. This image includes different types of noises, such as vehicle occlusion, sharp roadway curves, and building shadows.

The third image, which is shown in Figure 5(c), was collected by the WorldView satellite. The image shows an area in Shenzhen City, China. It has a spatial resolution of 0.6 m and a size of 3000 pixels × 1854 pixels. It includes various road conditions, such as road material changes, vehicle occlusion, and overhanging trees.

Figure 5 here

3.2 Experimental Setup and Parameter Setting

The accuracy and efficiency of the proposed road extraction method was investigated

through the following three experimental setups with three VHR remote sensing images shown above.

The first experiment aimed to investigate the accuracy and efficiency of the proposed method. For the fairness of comparison, we chose Miao's method (2014) and Gao's method (2018) as the comparison methods, because both methods need to rely on manually selected road seed points. Ground-truth datasets for the four images were interpreted manually, and are shown in Figures 6(a), 7(a)-7(b) and 8(a)-(b). Under the condition that the number and position of seed points are the same, three methods are used for road extraction respectively. The optimal parameters of each method are obtained by trial-and-error method. The parameter details of each approach are as follows: (1) In Miao's method, the threshold parameter was set at $T = 0.005$; (2) In Gao's method, the parameters were set as $T = 0.2$, $\alpha = 0.9$, $\beta = 0.9$, and $\lambda = 0.4$; (3) In the proposed method, the smooth term was set at $\lambda = 0.4$.

The second and third experiments were designed to verify the accuracy and advantages of the proposed method in complex urban environments (vegetation obscuration, dense vehicles, and building shadows, etc.). Two VHR satellite images were used in the experiments, as depicted in Figures 5(b) and 5(c). This design had two objectives. First, similar to the first and the second experiment, it aimed to test the efficiency of the proposed method. The second goal is to verify the robustness of the proposed road extraction method in the complex urban environment. We selected Miao's method (2014), Gao's method (2018) and Li's method (Li et al. 2015) as the comparison methods, of which the first two methods are the road centreline extraction method based on seed points, and the third method is the road region extraction method based on level set, requiring manual selection of the initial road region. The optimal parameters of each method are obtained by trial and error. The ground truth data set is collected manually, and the road centreline and the road surface are collected respectively. To ensure the fairness of the result comparison, when evaluating the accuracy, if the result extracted by the method is the road centreline, the linear road reference data will be selected for comparison; If the result extracted by this method is a road area, the planar road reference data will be selected for comparison. The parameters of these approaches were as follows: (1) In Miao's method, the threshold parameter was set at $T = 0.002$; (2) In Gao's method, the parameters were set as $T = 0.2$, $\alpha = 0.7$, $\beta = 0.7$, and $\lambda = 0.4$; (3) In Li's method, the scale parameter was set as $\sigma = 0.2$, time step was set as $\Delta t = 20$; (4) In the proposed method, the smooth term was set as $\lambda = 0.4$.

3.3 Experimental Results

On the basis of the experimental setup, we obtained the road extraction results by using different approaches. These methods are quantitatively compared using three measures: 1) Completeness, 2) Correctness, and 3) Quality(Wiedemann, Heipke, and Mayer 1998), as follows:

$$\text{Completeness} = \frac{\text{TP}}{\text{TP} + \text{FN}} \tag{18}$$

$$\text{Correctness} = \frac{TP}{TP + FP} \tag{19}$$

$$\text{Quality} = \frac{TP}{TP + FP + FN} \tag{20}$$

where TP, FN and FP represent true positive, false negative and false positive, respectively.

In this study, the ground truth datasets are obtained by hand-drawing method, including two data types of road centreline and road surface. If the accuracy of the road centreline is evaluated, the buffer width is set to 4 pixels. The buffer width is set to 0 pixels if the road surface is evaluated for accuracy.

In the first experiment, the proposed method was evaluated and compared with other approaches, including Miao's method (2014) and Gao's method (2018). Figure 6 illustrates the corresponding road extraction results. From Figure 6, it can be seen that both three methods can produce desired road connection topology. However, when the road material of seed points is different, the geodesic fails to produce correct results. By contrast, both Gao's method and the proposed method achieve the desired connection topology. This demonstrates that Gao's method and the proposed method cope with the road material change challenge.

Figure 6 here

In the second experiment (see Figure 7), we compared the method of Miao (2014), Gao (2018) and Li (2015) with the method we proposed. It can be seen from the figure that there are some omissions and errors in the extraction results of Miao's method, which mainly occurs when the road is blocked by a large shadow. The results obtained by Gao's method have good integrity, but some roads are not smooth enough. There are many false positives in the road surface extracted by Li's method, and many non-road areas are identified as road areas. We analyse the reason for this is that the distribution of ground objects in this image is more complex, and the road occlusion is more frequent. The method we proposed achieved satisfactory results. This is also verified from the statistics in Table 1. Roads extracted using our method have higher accuracy and extraction quality. This also reflects the advantages of our proposed approach.

Figure 7 here

Figure 8 here

The third experiment (see Figure 8) used a satellite image with a resolution of 0.6 meters. The area is covered with towering buildings and dense vegetation, as well as dense traffic on some sections. This poses a great challenge to road extraction. From the comparison of experimental results, it can be seen that there are some omission errors in the road extracted by Miao's method, and there are many errors in the road extraction in the shadow and the area covered by vehicles. The results extracted by Gao's method are not smooth enough and easy to deviate from the centre of the road.

The road extracted by Li's method has a lot of false alarms, mainly mixing the road with surrounding buildings without any difference. The results obtained by our method have better smoothness and are closer to the centre of the road. The statistics in Table 1 are also consistent with the extraction results shown in Figure 8. In general, the results extracted by the method based on seed point have higher quality than those extracted by the method based on level set.

Table 1 here

According to the aforementioned discussions, it can be seen that the proposed method provides a practical solution for accurate road centreline extraction from VHR satellite images with fewer interactions with users.

4. Discussion

4.1 Parameter Sensitivity Analysis

To test the smoothing value influence on the road centreline extraction accuracy, its value was adjusted automatically from 0.1 to 0.6 with an increment of 0.1 for each step. The test results are presented in Figure 9. The performance of the smoothing value influence is quantitatively evaluated in terms of three accuracy measures, 1) Completeness, 2) Correctness, and 3) Quality.

Figure 9 here

Figure 10 reports quantitative evaluation results with different smoothing values. From Figure 10, it can be seen that, when the smoothing value is increased from 0.1 to 0.4, the accuracy is slightly changed. However, the accuracy is decreasing when the smoothing value is exceeding 0.4. The reason for this phenomenon is that the large smoothing value cannot produce the complete road buffer, as shown in Figures 9(e) and 9(f). To achieve the best accuracy, this study fixed the length term to 0.4 throughout the tests.

Figure 10 here

4.2 Computational Cost Analysis

In this section, we present a discussion of the computational cost of the proposed approach. This study used MATLAB® (R2010b version) as the coding environment on a PC that had an Intel Core 2 Quad processor with a 2.83-GHz clock speed.

For the road extraction algorithm based on seed points, in order to eliminate the influence of the number and location of seed points on the algorithm, we used the same number and location of seed points in the process of road extraction with different methods, and calculated the time required by each algorithm. These seed points were

obtained manually during the process of making reference data. The statistical results are shown in Table 2. According to the statistical results, in the case of using the same number and location of seed points, the method of Miao (2014) requires the least time, and the method of Gao (2018) consumes the most time. However, the proposed method requires the same time as Miao's method when the number of seed points is small, and the time required is between Miao's method and Gao's method when the number of seed points is large. Combined with the statistical data in Table 1, it can be seen that on the premise of ensuring the accuracy and quality of the extraction results, the method proposed has higher extraction efficiency.

Table 2 here

5. Conclusion

This study has proposed a semi-automatic method for road centreline extraction from Very High Resolution (VHR) satellite images. By using colour transformation, the proposed method is able to tackle the illumination variance caused by the road material change. Benefited from the kernel density estimation method, the proposed method can produce more centred roads than the geodesic method. Compared to existing methods in the literature, the proposed method can produce similar extraction accuracy with fewer interactions with users. Experimental results demonstrate that the proposed method provides a practical and reliable solution for semi-automatic road centreline delineation from VHR satellite images.

ACKNOWLEDGEMENT

The authors would like to thank the editor-in-chief, the anonymous associate editor, and the reviewers for their insightful comments and suggestions. This work was partly supported by the National Key Research and Development Program (2018YFA0605504), the National Natural Science Foundation of China (41701500, 41601440, and 41601354), the Natural Science Foundation of Hunan Province (2018JJ3641), the Scientific Research Foundation for Distinguished Scholars, Central South University (502045001) and Project of Urban Spatial Information Infrastructure for Smart City, The Hong Kong Polytechnic University (1-ZEAB).

REFERENCES

Ahamada, Ibrahim , and Emmanuel, Flachaire. 2010. *Non-Parametric Econometrics*, Oxford: Oxford University.

Chai, D. F., W. Forstner, and F. Lafarge. 2013. Recovering Line-Networks in Images by Junction-Point Processes. In Proceedings of the IEEE Computer Society Conference on Computer Vision and Pattern Recognition. Oregon, Portland, June 25–27, pp. 1894-1901.

Chan, T. F., and L. A. Vese. 2001. Active contours without edges. *IEEE Transactions on Image Processing*, **10**, pp. 266-277.

Dal Poz, A. P., R. A. B. Gallis, J. F. C. da Silva, and E. F. O. Martins. 2012. Object-space road extraction in rural areas using stereoscopic aerial images. *IEEE Geoscience and Remote Sensing Letters*, **9**, pp. 654-658.

Das, S., T. T. Mirnalinee, and K. Varghese. 2011. Use of salient features for the design of a multistage framework to extract roads from high-resolution multispectral satellite images. *IEEE Transactions on Geoscience and Remote Sensing*, **49**, pp. 3906-3931.

Gao, L.P., W. Z. Shi, Z. L. Miao, and Z. Y. Lv. 2018. Method Based on Edge Constraint and Fast Marching for Road Centerline Extraction from Very High-Resolution Remote Sensing Images. *Remote Sensing,* **10 (6),** pp. 900.

Gonzalez, Rafael C., Richard E. Woods, and Steven L. Eddins. 2003. *Digital Image Processing Using MATLAB*, Prentice-Hall, Inc.

Hu, X. Y., Z. X. Zhang, and C. V. Tao. 2004. A robust method for semi-automatic extraction of road centerlines using a piecewise parabolic model and least square template matching. *Photogrammetric Engineering and Remote Sensing*, **70**, pp. 1393-1398.

Li, Z. B., W. Z. Shi, Q. M. Wang, and Z. L. Miao. 2015. Extracting Man-Made Objects From High Spatial Resolution Remote Sensing Images via Fast Level Set Evolutions. *IEEE Transactions on Geoscience and Remote Sensing*, **53 (2)**, pp. 883-899.

Lin, X. G., J. X. Zhang, Z. J. Liu, J. Shen, and M. Y. Duan. 2011. Semi-automatic extraction of road networks by least squares interlaced template matching in urban areas. *International Journal of Remote Sensing*, **32**, pp. 4943-4959.

Lv, Z., Y. H. Jia, Q. Zhang, and Y. F. Chen. 2017. An Adaptive Multifeature Sparsity-Based Model for Semiautomatic Road Extraction From High-Resolution Satellite Images in Urban Areas. *IEEE Geoscience and Remote Sensing Letters,* **14 (8)**, pp. 1238-1242.

Mena, J. B. 2003. State of the art on automatic road extraction for GIS update: a novel classification. *Pattern Recognition Letters*, **24**, pp. 3037-3058.

Miao, Z. L., B. Wang, W. Z. Shi, and H. Zhang. 2014. A Semi-Automatic Method for Road Centerline Extraction From VHR Images. *IEEE Geoscience and Remote Sensing Letters,* **11 (11)**, pp. 1856-1860.

Osher, S., and R. P. Fedkiw. 2001. Level set methods: An overview and some recent results. *Journal of Computational Physics*, **169**, pp. 463-502.

Peyré, Gabriel, Mickael Péchaud, Renaud Keriven, and Laurent D. Cohen. 2010. Geodesic methods in computer vision and graphics. *Foundations and Trends in Computer Graphics and Vision*, **5**, pp. 197-397.

Poullis, C., and S. Y. You. 2010. Delineation and geometric modeling of road networks. *ISPRS Journal of Photogrammetry and Remote Sensing*, **65**, pp. 165-181.

Scott, David W. 2015. *Multivariate density estimation: theory, practice, and visualization*, New York, Chichester: Wiley.

Turetken, E., G. Gonzalez, C. Blum, and P. Fua. 2011. Automated reconstruction of dendritic and axonal trees by global optimization with geometric priors. *Neuroinformatics*, **9**, pp. 279-302.

Vese, L. A., and T. F. Chan. 2002. A multiphase level set framework for image segmentation using the Mumford and Shah model. *International Journal of Computer Vision*, **50**, pp. 271-293.

Wegner, J. D., J. A. Montoya-Zegarra, and K. Schindler. 2015. Road networks as collections of minimum cost paths. *ISPRS Journal of Photogrammetry and Remote Sensing*, **108**, pp. 128-137.

Wiedemann, C., C. Heipke, and H. Mayer. 1998. Empirical evaluation of automatically extracted road

axes. Paper presented at the Proc. CVPR Workshop Empirical Eval. Methods Comput., Los Alamitos, CA.

Zhang, J. X., X. G. Lin, Z. J. Liu, and J. Shen. 2011. Semi-automatic road tracking by template matching and distance transformation in urban areas. *International Journal of Remote Sensing* **32**, pp. 8331-8347.

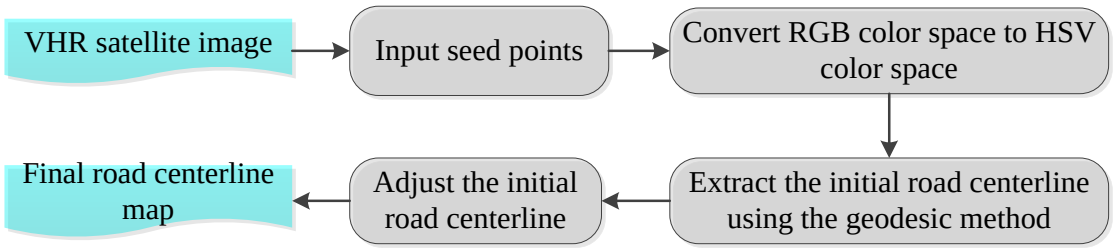

Figure 1. Flowchart of the proposed method.

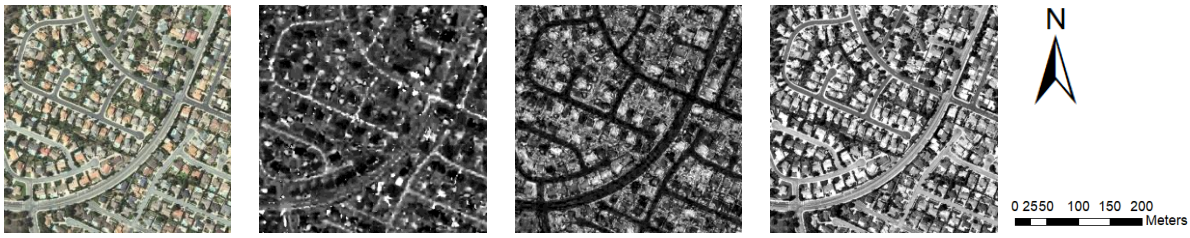

(a) (b) (c) (d)

Figure 2. An example of colour transformation. (a) The RGB image, (b) the hue component, (c) the saturation component, (d) the value component (i.e. brightness).

(a) (b) (c)

Figure 3. (a) Seed points are shown in blue cross. (b) The geodesic method connection result which is shown in red. (c) The superposition result of the geodesic result and the original test image.

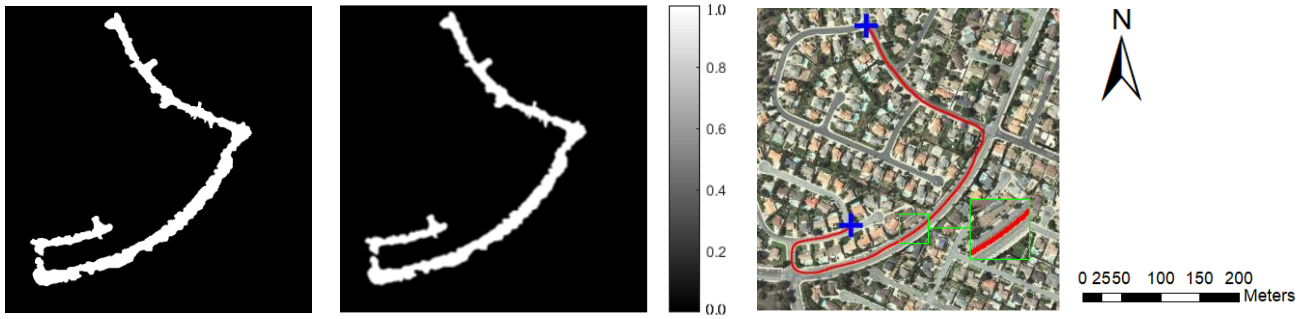

(a) (b) (c)

Figure 4. The centreline adjustment result. (a) The road buffer constructed by active contour, the *road* class is shown in 'white' while the *non-road* class in 'black', (b) The road centreline probability estimated by KDE, (c) The initial road centreline adjustment result using the geodesic method. The road centreline is shown in red.

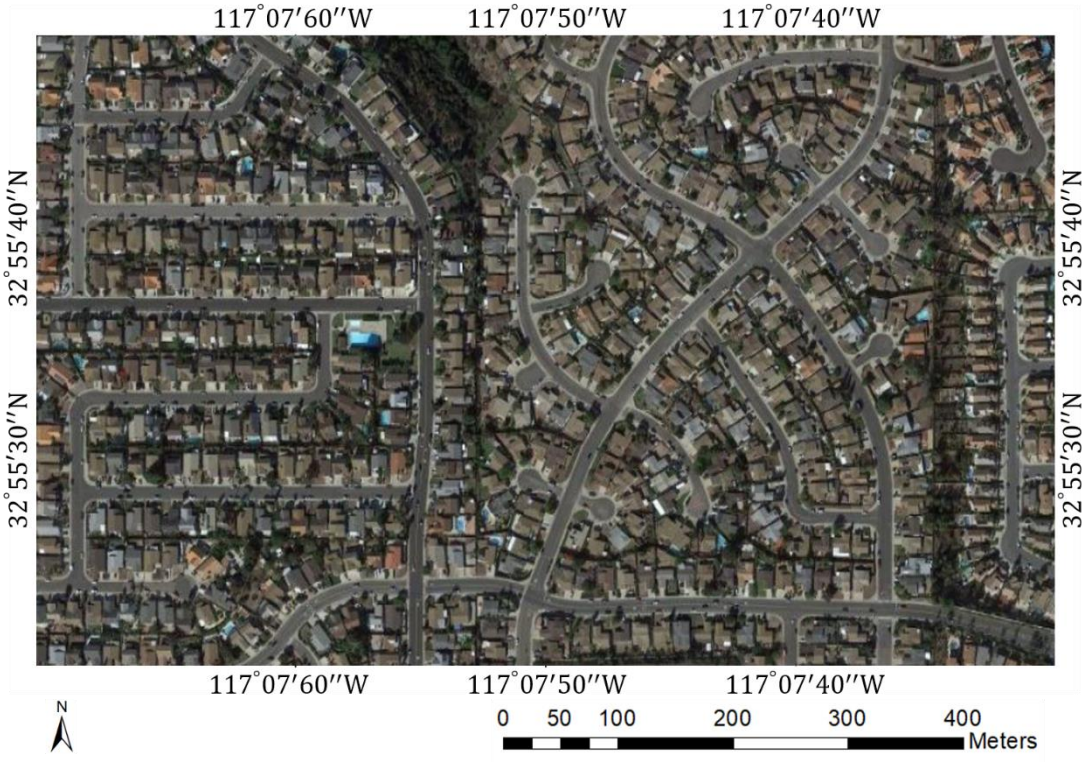

(a)

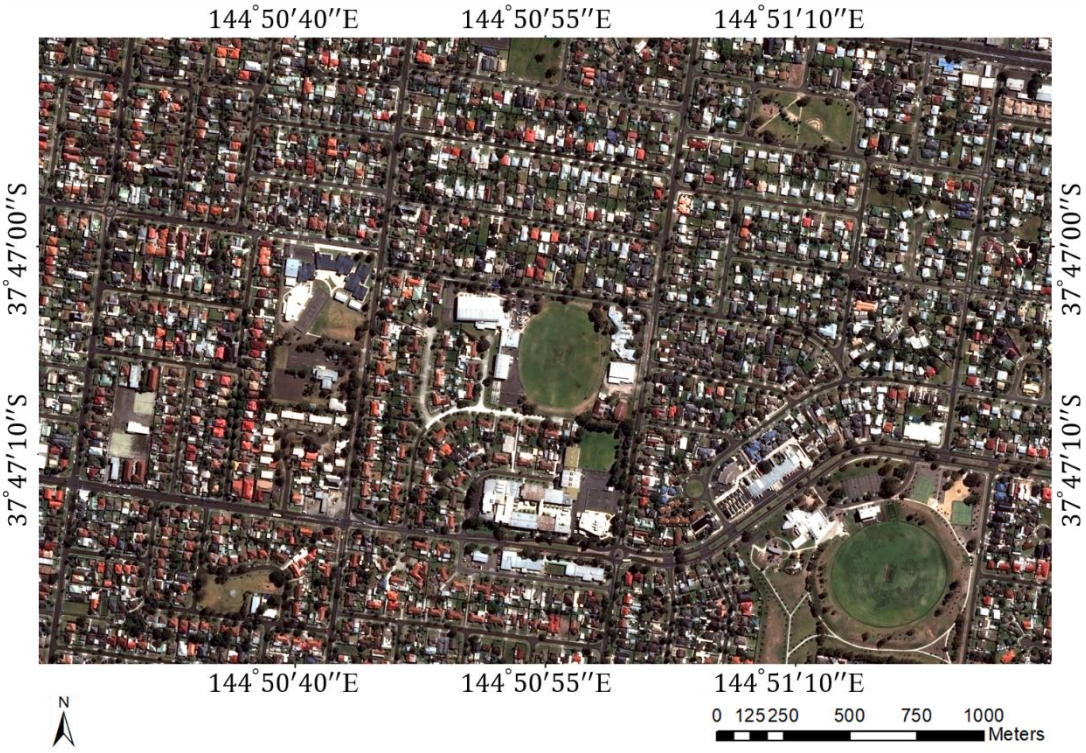

(b)

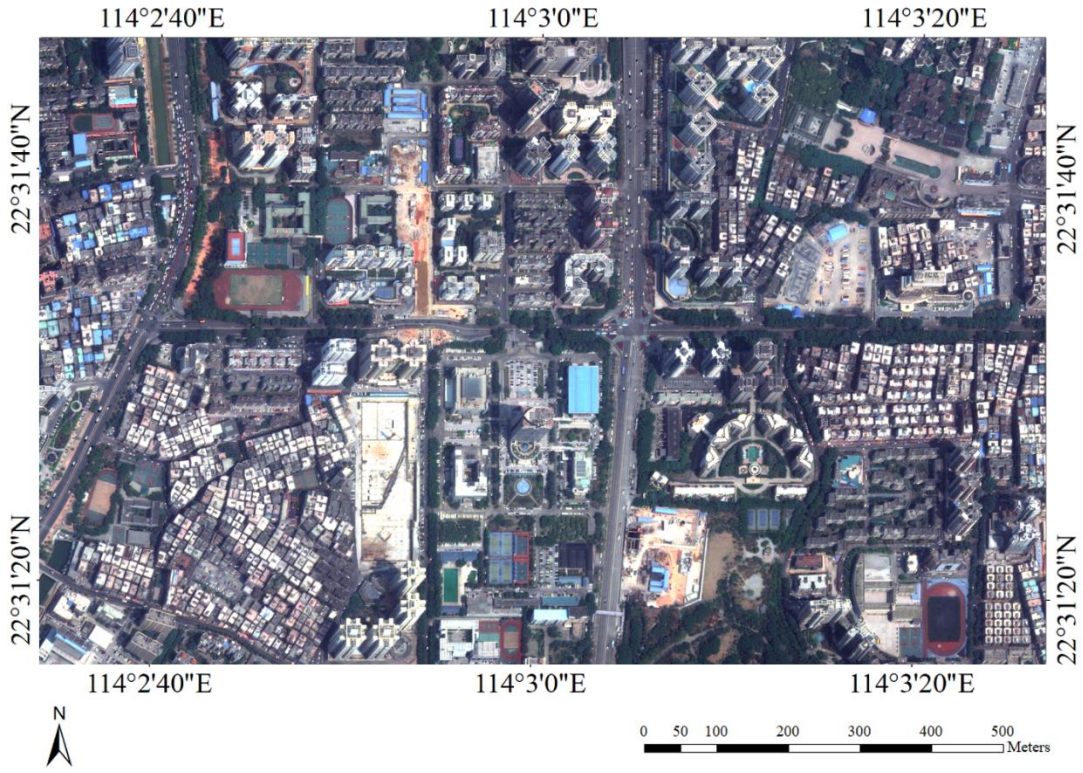

(c)

493 Figure 5. Test images used in this study.

494

495

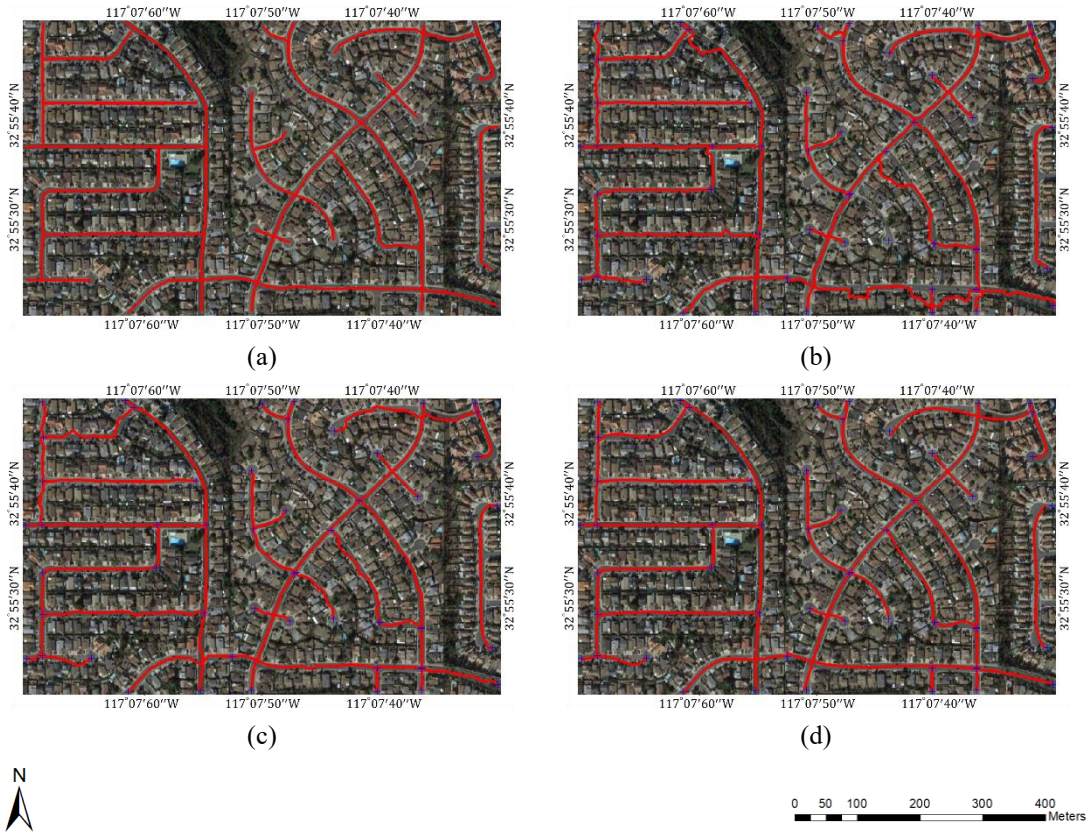

Figure 6. Results of experiment 1. (a)Reference road centreline, (b) Miao's method, (c) Gao's method, (d) The proposed method. Seed points are shown in blue cross and the road centrelines are shown in red.

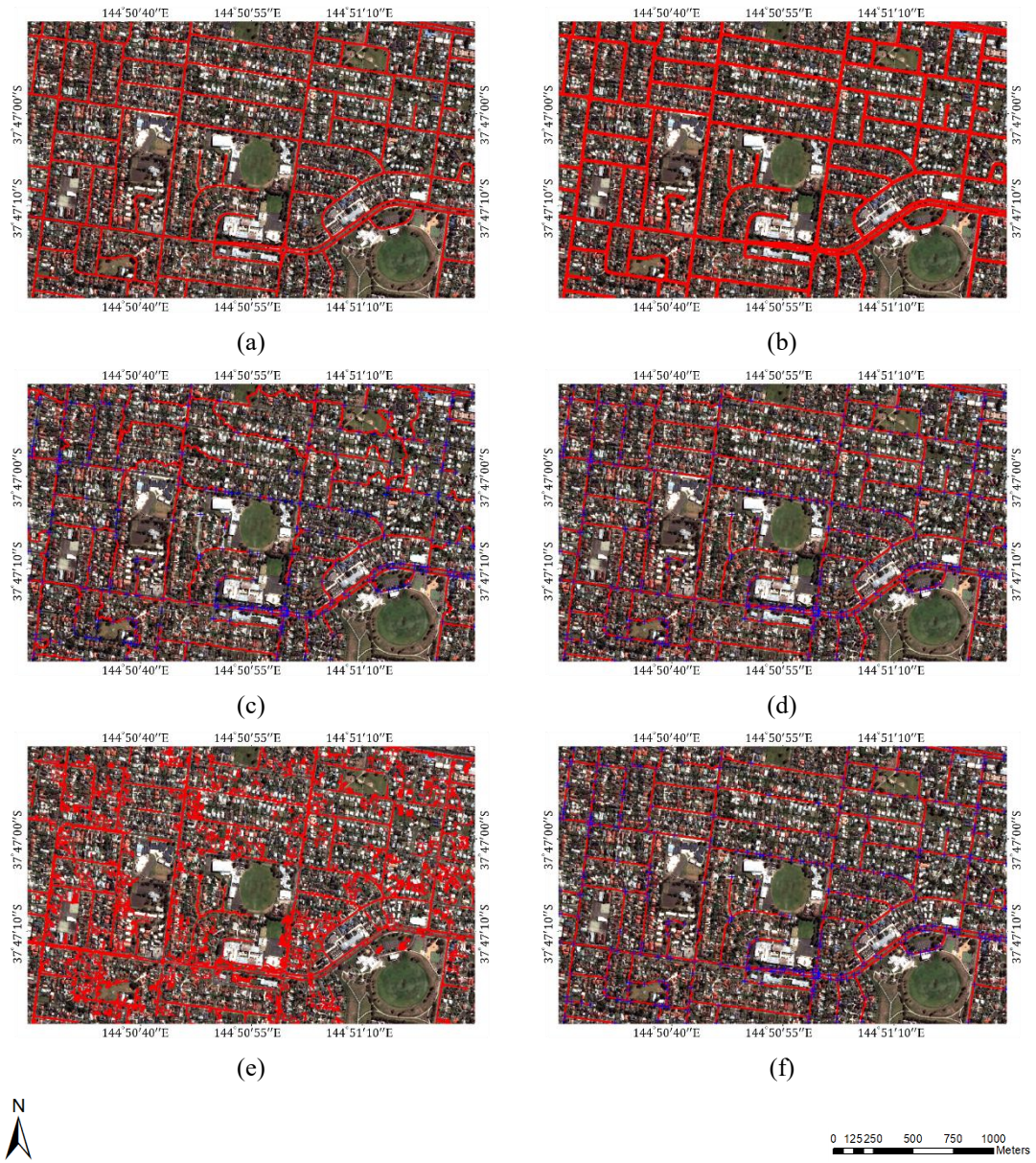

Figure 7. Results of experiment 2. (a)Reference road centreline, (b) Reference road area, (c) Miao's method, (d) Gao's method, (e) Li's method, (f) The proposed method. Seed points are shown in blue cross and the road centrelines are shown in red.

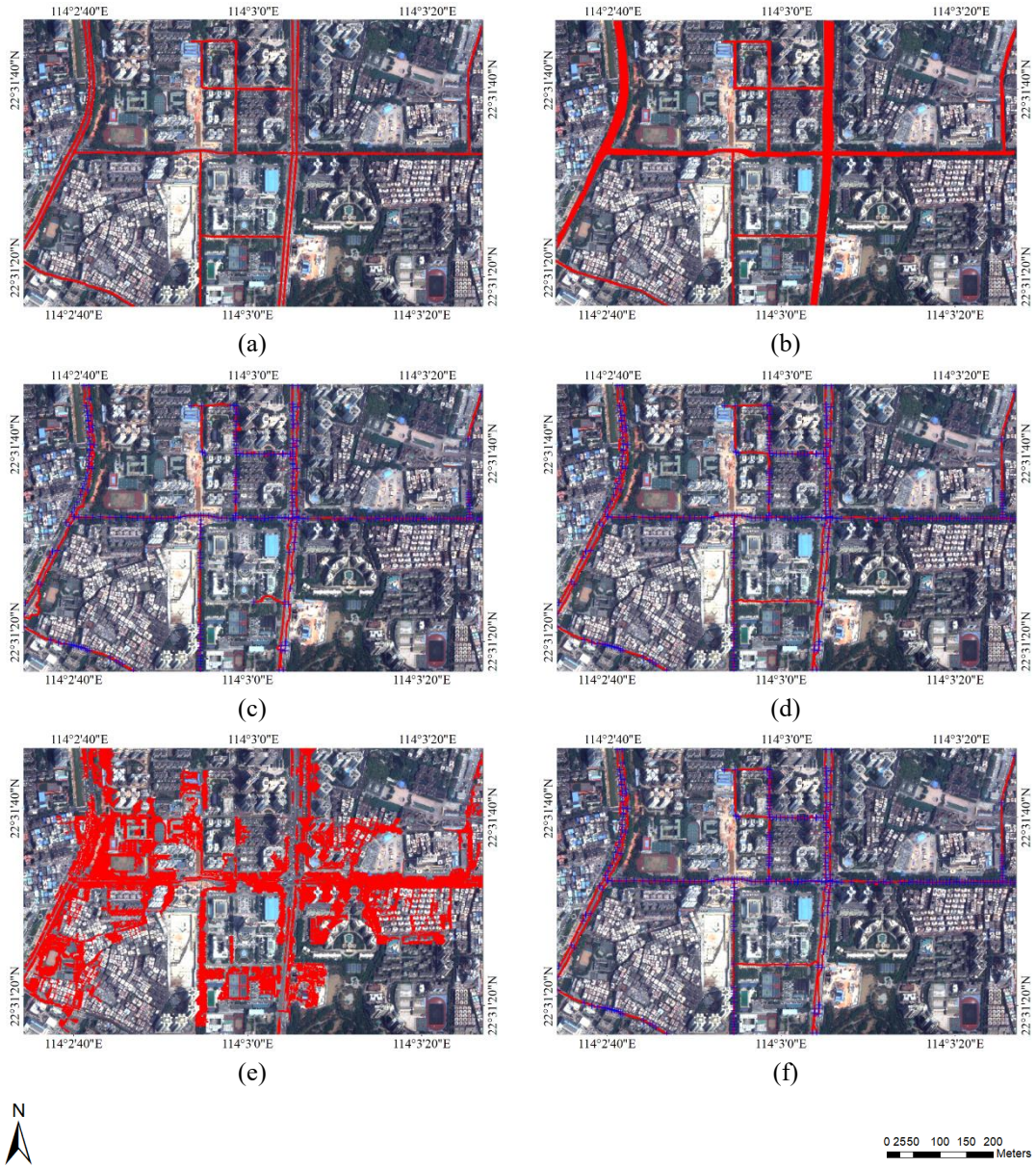

Figure 8. Results of experiment 3. (a)Reference road centreline, (b) Reference road area, (c) Miao's method, (d) Gao's method, (e) Li's method, (f) The proposed method. Seed points are shown in blue cross and the road centrelines are shown in red.

Table 1 Comparison of different semi-automatic road centreline extraction methods

Method	Completeness (%)	Correctness (%)	Quality (%)
Experiment 1			
Miao's method	88.59	83.42	75.33
Gao's method	92.33	88.29	82.26
Proposed	91.03	90.58	83.17
Experiment 2			
Miao's method	64.15	65.01	47.68
Gao's method	95.17	92.70	88.53
Li's method	50.60	44.89	31.21
Proposed	94.54	93.34	88.57
Experiment 3			
Miao's method	73.58	77.27	60.49
Gao's method	88.43	83.81	75.52
Li's method	51.84	15.66	13.67
Proposed	87.53	85.02	75.84

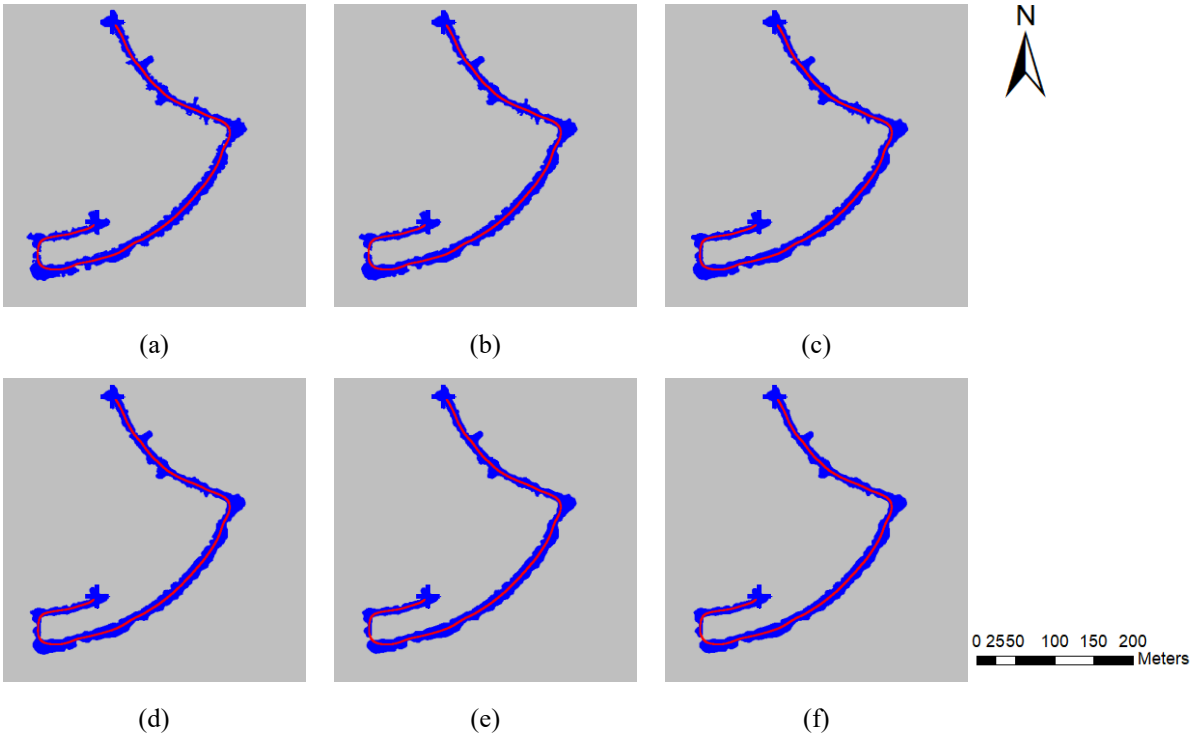

Figure 9. Road centreline extraction results with different smoothing values. (a) 0.1. (b) 0.2. (c) 0.3. (d) 0.4. (e) 0.5. (f) 0.6. The pixels in the road buffer extracted by level set are shown in blue while the corresponding road centreline in red.

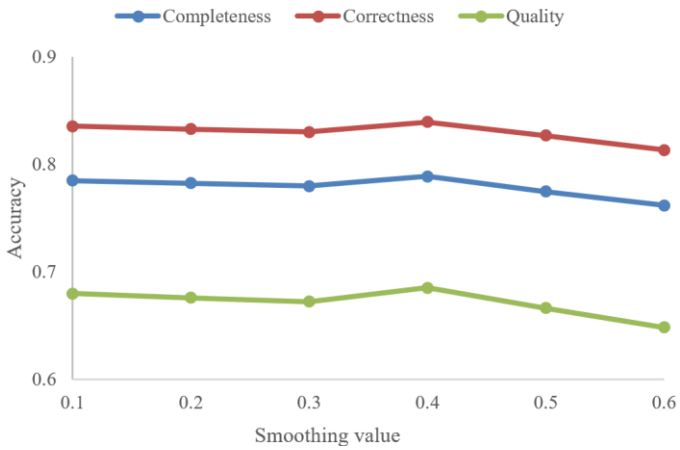

Figure 10. The quantitative evaluation result of the smoothing value influence on accuracy.

Table 2 Computation Cost of Different Centreline Extraction Methods

	Miao *et al.*'s method (2014)	**Gao *et al.*'s method (2018)**	**Proposed method**
Experiment 1			
Time (s)	37	47	45
Number of seed points	54	54	54
Experiment 2			
Time (s)	988	1567	1324
Number of seed points	455	455	455
Experiment 3			
Time (s)	327	986	423
Number of seed points	370	370	370